

Band Structure and Polarization Effects in Photothermoelectric Spectroscopy of a Bi₂Se₃ Device

Seyyedesadaf Pournia,¹ Giriraj Jnawali,¹ Ryan F. Need,^{2,3} Howard E. Jackson,¹ Stephen D. Wilson,² and Leigh M. Smith,^{*,1}

¹ *Department of Physics and Astronomy, University of Cincinnati, Cincinnati, OH 45221, USA.*

² *Materials Department, University of California, Santa Barbara, CA 93106, USA*

³ *Department of Materials Science and Engineering, University of Florida, Gainesville, FL 32611, USA*

** Author to whom correspondence should be addressed: leigh.smith@uc.edu*

Abstract

Bi₂Se₃ is a prototypical topological insulator which has a small band gap (~0.3 eV) and topologically protected conducting surface states. This material exhibits quite strong thermoelectric effects. Here we show in a mechanically exfoliated quasi-bulk nanoflake device that we can measure the energy dependent optical absorption through the photothermoelectric effect. Spectral signatures are seen for a number of optical transitions between the valence and conduction bands, as well as the 1.5 eV optical transition between the two topologically protected conducting surface states. We also observe a surprising linear polarization dependence in the response of the device that reflects the influence of the metal contacts.

KEYWORDS: Bi₂Se₃, optical transition, photothermoelectric effect, band gap

The novel properties of the nontrivial surface states in Bi_2Se_3 and other three dimensional topological insulators have led to the prediction and discovery of unique optical effects such as the circular photogalvanic effect (CPGE) and the photoinduced inverse spin Hall effect (PISHE) in the near-infrared and mid-infrared.¹⁻⁸ However, this material has also been seen as a promising thermoelectric material, with the ability to convert heat into electricity.⁹⁻¹⁴ At the same time, bulk Bi_2Se_3 is a standard semiconductor that possesses allowed optical transitions between the occupied valence bands to the unoccupied conduction bands.¹⁵ In this letter we consider the photosensitivity of a single device fabricated from a quasi-bulk nanoflake which is mechanically exfoliated from a single crystal. We show that the photoresponse is dominated by the photothermoelectric effect through a temperature gradient caused by the absorption of the excitation laser. Significant polarization effects are also seen that are due to the presence of the metallic contacts.

Single crystals of Bi_2Se_3 were grown using the Bridgeman method from stoichiometric elements as described elsewhere.¹⁵ The bulk crystals were degenerately doped n-type ($N_D \sim 10^{19} \text{ cm}^{-3}$). Relatively thick ($\sim 200 \text{ nm}$) nanoflakes were exfoliated using the scotch tape method and transferred to a high purity p-type silicon substrate with a 300 nm thermal oxide layer. After visualization of the nanoflakes using a microscope, Ti/Al (20 nm/300 nm) contacts with $\sim 5 \mu\text{m}$ gap were defined across the nanoflakes using photolithography followed by e-beam deposition of a Ti/Al thin film and liftoff. After confirming that the contacts were ohmic using I-V measurements in a probe station, the device was mounted into a chip carrier and wires bonded to the contacts. The assembly was mounted to the copper cold finger in the vacuum space of a ST-500 Janis microscope cryostat with an Attocube piezoelectric xy-scanner for fine positioning and a thin CaF_2 infrared window for conducting the optical experiments. The temperature could be varied between 10 K and 300 K. Transport measurements were implemented using a SRS variable constant current source and measuring the change in the bias.

The tunable output of an optical parametric oscillator pumped by a pulsed (150 fs/80 MHz) Ti-sapphire laser was used to photoexcite the device over a continuous energy range extending from 0.3 eV (4050 nm) to 1.8 eV (680 nm). A 40 \times /0.5 N.A. protected silver reflective objective was used to focus the laser beam to a diffraction-limited spot onto the sample (\sim 1 to 5 μ m, depending on wavelength). The average power could be varied between 150 and 750 μ W ($P_0/5$ and P_0 , respectively), and the orientation of the linear polarization relative to the contacts could be controlled using a CaF₂ double Fresnel rhomb rotator.

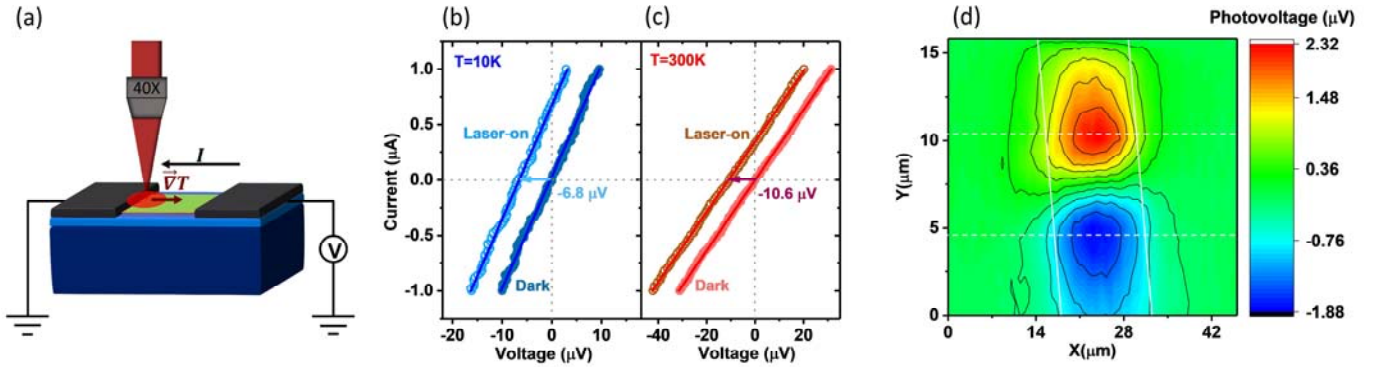


FIG. 1. (a) Schematic diagram of the experiment. I-V measurements at (b) 10K and at (c) 300K in the dark and under 1.16 eV (1070 nm) illumination with power of P_0 . (d) 2D mapping of the device photoresponse with a power of $P_0/5$ at 300 K. Solid lines show approximate edges of Bi₂Se₃ nanoflake, while dashed lines show approximate edges of metallic contacts.

Figure 1(a) shows a schematic diagram of a photocurrent measurement in a Bi₂Se₃ nanoflake device. With the laser positioned close to one contact, current-voltage (I-V) measurements are shown at 10 K (Fig. 1(b)) and 300 K (Fig. 1(c)) in the dark and under 1.16 eV (1070 nm) laser illumination. The I-V measurements are clearly linear indicating that the metal-semiconductor contacts are ohmic. The resistance of the device is 31 Ω at 300 K and 10 Ω at 10 K which, since the resistance of the device decreases with temperature, exhibits metallic behavior. Given the thickness of the flake (\sim 200 nm) with the distance

between the contacts ($\sim 5 \mu\text{m}$) and the width of the flake ($\sim 15 \mu\text{m}$), we calculate that the resistivity of the Bi_2Se_3 is $1.6 \times 10^{-3} \Omega\cdot\text{cm}$ at 300 K and $5 \times 10^{-4} \Omega\cdot\text{cm}$ at 10 K. Considering the average literature values for mobility in similar n-type (metallic) Bi_2Se_3 devices, $\mu_{300\text{K}} = 550 \text{ cm}^2/\text{V}\cdot\text{s}$ and $\mu_{10\text{K}} = 1800 \text{ cm}^2/\text{V}\cdot\text{s}$,¹⁶⁻¹⁸ we find the free carrier density to be $n_{3D} = 7 \times 10^{18} \text{ cm}^{-3}$, which is in agreement with the result of the transient reflectivity (TR) measurement on a nanoflake exfoliated from the same bulk crystal.¹⁵ This carrier density indicates a highly doped sample, which has been seen in similar crystals grown using the growth method described previously.¹⁵

Under illumination with $750 \mu\text{W}$ of 1.16 eV (1070 nm) light, the slope of the I-V curve does not change demonstrating that the resistivity does not change under illumination. If we assume all of the light is absorbed by the flake, the expected photoexcited pair density is less than 10% of the background electron density in steady state assuming an average lifetime of 150 ps and a spot size of $\sim 2 \mu\text{m}$.¹⁵ On the other hand, the I-V profile is shifted by $6.8 \mu\text{V}$ at 10 K and by $10.6 \mu\text{V}$ at 300 K from the measurements in the dark. This rigid shift indicates that while the conductivity does not change, a voltage across the contacts is induced by the illumination of the laser. Assuming that the power is completely absorbed near one contact (*cf.* Fig. 1(a)) the laser creates a temperature gradient across the device which in turn induces a voltage across the contacts through the Seebeck effect. This phenomena is known as the photothermoelectric effect (PTE),^{19,20} in which illumination drives current flow under short circuit ($V = 0$) conditions, or creates a potential difference between the two electrodes (ΔV_{PTE}) under open circuit ($I = 0$)¹⁹ conditions. The magnitude of the photothermoelectric effect depends on the Seebeck coefficient, which in turn depends on the conductivity of the sample near the Fermi energy, and the temperature gradient induced between the two ends of the

material. The temperature gradient in steady state is determined by the amount of energy absorbed at one end, and the thermal conductivity of the material.

The conclusion that PTE drives the photoresponse is supported by the photocurrent map shown in Figure 1(d) which displays how the induced voltage at constant current ($I = 0$) varies as a function of the position of the laser. The dotted lines show the edges of the metal contacts and solid lines show the edges of the Bi_2Se_3 nanoflake. The power of the 1.16 eV laser was $P_0/5 = 150 \mu\text{W}$ with a spot size of $1.4 \mu\text{m}$ in this image determined by the numerical aperture (0.5) of the reflective objective. The maximum induced voltage is seen when the laser is positioned at the edge of the metal contacts which would be expected to create the largest temperature gradient across the flake. The voltages are positive when the laser is near one contact and negative when it is near the other because the temperature gradient reverses sign. Prior measurements of similar Bi_2Se_3 material have shown the Seebeck coefficient to range from $51 - 82 \mu\text{V/K}$,²¹⁻²³ which suggests a $\sim 34 \text{ mK}$ temperature difference between the two ends of the flake, for $\Delta V_{PTE} = 2.32 \mu\text{V}$ (Fig. 1(d)) and assuming all of the incident $P_0/5 = 150 \mu\text{W}$ is absorbed by the material. The induced voltage midway between the contacts is zero since there is no temperature gradient in that case.

Interestingly, the induced voltage is relatively constant when the flake is illuminated through the aluminum contacts. This indicates that the absorbed power does not change appreciably when the laser is over the contacts, but also indicates that the temperature is relatively constant for the flake underneath the contacts (with a negligibly small temperature gradient), resulting in a temperature gradient which is maximum between the contacts. The small thermal gradient under the contacts is consistent with the high thermal conductivity of the aluminum relative to the underlying Bi_2Se_3 resulting in a nearly constant temperature no matter where the laser spot is located on the metal film.

At constant current (here $I = 0$), the potential induced by PTE depends on the induced temperature gradient between the contacts, which depends on the amount of laser power absorbed by the nanoflake. It should thus be possible to measure how the absorption changes in the Bi_2Se_3 with energy. Figure 2(b) shows the induced photovoltage in the device as a function of photon energy from 0.3 to 1.8 eV (4000 nm – 680 nm) at 300 K (red spectrum) and 10 K (blue spectrum). The laser was focused on a point close to the metal contact with the maximum photoresponse. Here, the photoresponse of the device has been normalized by the power of the laser, $(\Delta V_{PTE}/P)$, for each single wavelength in order to obtain a measure of how the absorption changes with wavelength. The photovoltage spectra in Fig. 2(b), shows three peaks at 0.36 eV, 1.1 eV and 1.51 eV noted by blue bands. A schematic of the band structure of the material and carrier transitions related to the energy peaks of the spectra is depicted in Fig. 2(a). After a rapid onset beginning at 0.32 eV, the peak at 0.36 eV is the optical band gap determined by optical transitions between the uppermost valence band (VB_1) and the Fermi level (E_f) in the conduction band determined by the electron doping density. Previous transient reflectivity measurements in a similar flake have shown that the fundamental gap is ~ 0.2 eV with a Fermi energy of 120 meV which matches the onset observed at 0.32 eV.^{24,25} The second peak at 1.1 eV, is the energy required to excite the carriers from the second valence band (VB_2) to the Fermi level and was also resolved in the TR measurements on a similar nanoflake.²⁶ The third broad peak centered at 1.51 eV (820 nm) is the well-known optical transition between the first to second Dirac surface states expected in a Bi_2Se_3 topological insulator.²⁷ This resonance has been confirmed experimentally²⁸ and most CPGE measurements on this TI material are performed at this energy.^{1,4}

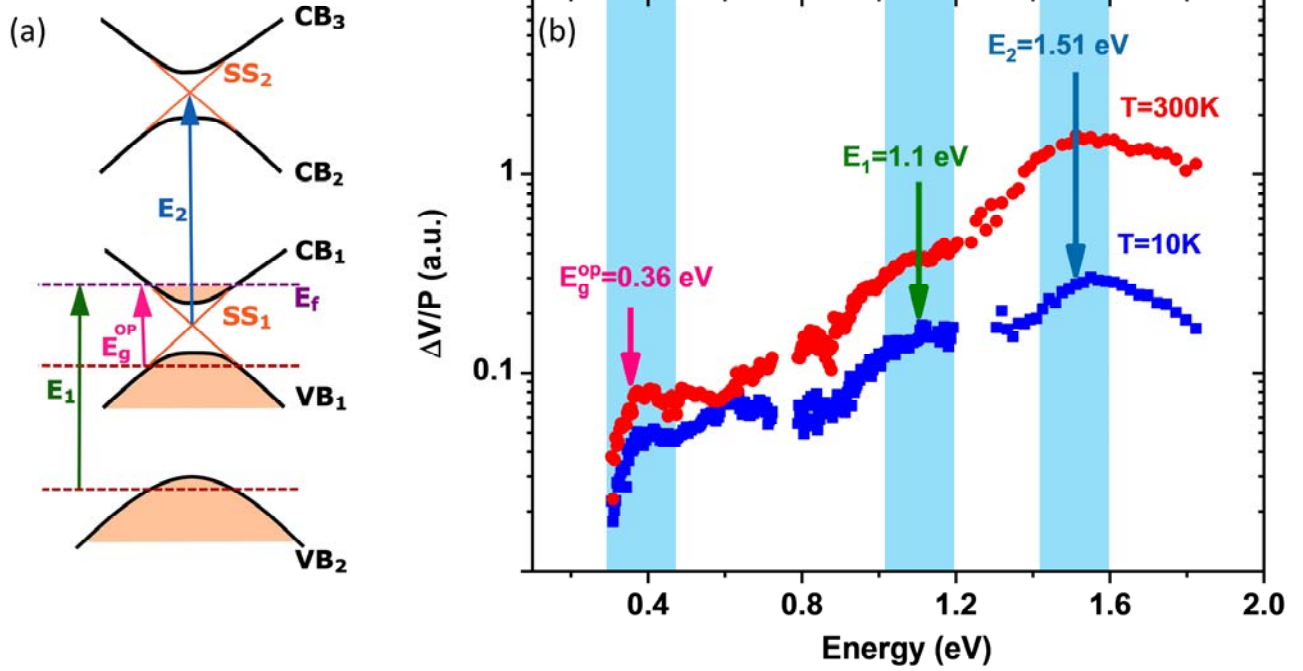


FIG. 2. (a) Schematic of the Bi₂Se₃ energy band structure with optical transitions noted by vertical arrows. (b) The induced photovoltage spectra at 300K (red) and 10K (blue). Spectral features are shown by shaded vertical bars noting the optical transitions for (E_g) the optical gap, (E_1) the transition from the second VB to the Fermi level in the CB, and (E_2) the transition from the first SS1 to second Dirac surface states SS2.

The energy-dependent measurements in Fig. 2 are consistent with the expected dependence of the absorption in this material. We now discuss how we can understand this detection mechanism based on the Seebeck effect. The temperature gradient induced by the laser (dT/dx) can be determined by Eq. 1 which shows that the rate at which heat is deposited in the sample (dQ/dt) is balanced by the transport of heat away from the excitation point, which in turn is determined by the thermal conductivity, κ , and the cross-sectional area of the flake.²⁹ The absorbed power (dQ/dt) is also equal to the energy dependent absorption coefficient $\alpha(\mathcal{E})$ times the incident laser power P , leading to Eq. 2.

$$\frac{dQ}{dt} = -A \kappa \frac{dT}{dx} \quad (1)$$

$$\alpha(E)P = -A \kappa \frac{dT}{dx} \quad (2)$$

However, the PTE voltage is directly proportional to the temperature gradient through the Seebeck coefficient, $\Delta V_{PTE} = -S \Delta T$ and so $\Delta V/P \sim \alpha$. Thus, we can conclude that $\Delta V/P$ as a function of photon energy is a direct measure of the energy-dependent absorption.

Notably, we have found that the maximum photovoltage depends on the orientation of the laser polarization relative to the contact. This is unexpected since the absorption coefficient along the a or b crystallographic directions for Bi_2Se_3 should not depend on polarization (i.e., the response should be isotropic). For Bi_2Se_3 with rhombohedral crystal structure and a hexagonal surface, the absorption coefficients along a and b crystal axes should be the same by symmetry. Figure 3(a) shows the photovoltage under constant 1070 nm wavelength illumination as a function of laser polarization. The induced photovoltage is clearly maximum for a polarization perpendicular to the electrode (parallel to the current), which means that the temperature gradient is larger which means the absorbed power is also larger. We can fit the polarization dependence of the photovoltage as $\Delta V = D + L \cos(2\varphi)$, where D is the polarization independent response, L is the polarization dependent term which is equal to about 15 % of D , and φ is the polarization angle with respect to perpendicular to the contact. The red (blue) profile is for the measurements close to the top (bottom) contact in Fig. 1(d). This result clearly shows that the positive or negative current is optimized for the polarization aligned with the current, and is about 25% less for the polarization perpendicular to the current or parallel to the contacts.

Bi_2Se_3 exhibits a polarization dependent linear photogalvanic effect (LPGE) but this occurs only for laser illumination not at normal incidence but at an angle. Furthermore, it should not depend on the spatial

position of the laser. We do not see any polarization dependence (or signal) midway between the contacts where the PTE signal is zero. We conclude that the polarization dependence must come from the contacts.

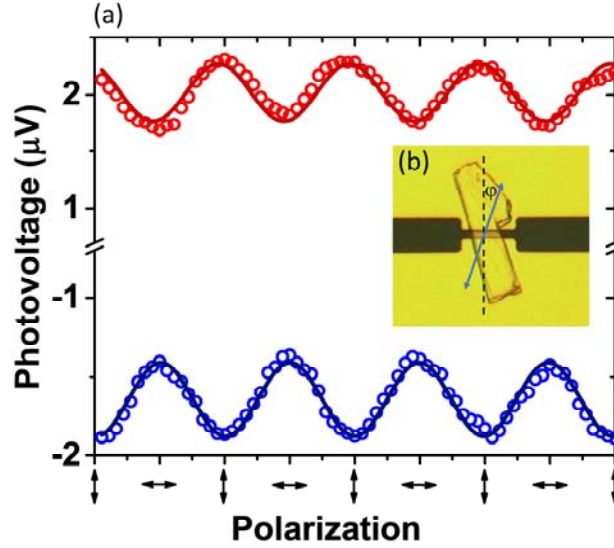


FIG. 3. (a) Linear polarization dependence of the photothermoelectric (PTE) response. (b) Optical image of the Bi₂Se₃ device used in this experiment and the schematic polarization vector orientation with respect to the normal of the contact edges.

To support this conclusion, we simulated the anisotropic effect of the contacts using the FDTD calculator program Lumerical. As shown in Fig. 4, when 1070 nm laser illumination is focused well away from the contact ($x = 1.5 \mu\text{m}$ and $y = 1.5 \mu\text{m}$), the square of the electric field (E^2) has no polarization dependence. However, when the laser is focused directly on the edge of the contact ($x = 1.5 \mu\text{m}$ and $y = 4.5 \mu\text{m}$), E^2 (and so α) is larger for the linear polarization perpendicular to the metal contact (parallel to the induced current). This response can be completely understood by considering the boundary conditions for the electric field at the edge of a metal contact. For a perfect metal, the tangential electric field must be zero at the interface for continuity, while the perpendicular component of the electric field induces a surface

charge which allows a discontinuous transition to zero field inside the metal. The transition is limited to the skin depth. The depletion of the electric field at the interface for parallel polarization is caused by the fact that it must go to zero inside the metal. Indeed, this depletion is seen as the electric field is measured within 200 nm of the interface, even though the laser spot (the maximum of the incident intensity) is located directly on the interface. On the other hand, for perpendicular polarization, the field strength is also clearly perturbed causing a slight 8% strengthening of the field intensity at the interface, and a more rapid falloff of the strength with distance. Both of these effects are responsible for the observed polarization dependence. One can estimate the degree of linear dichroism to be $\sim 25\%$ by estimating the maximum intensities for each polarization from the FDTD calculation. This is consistent with the measured value of 25%.

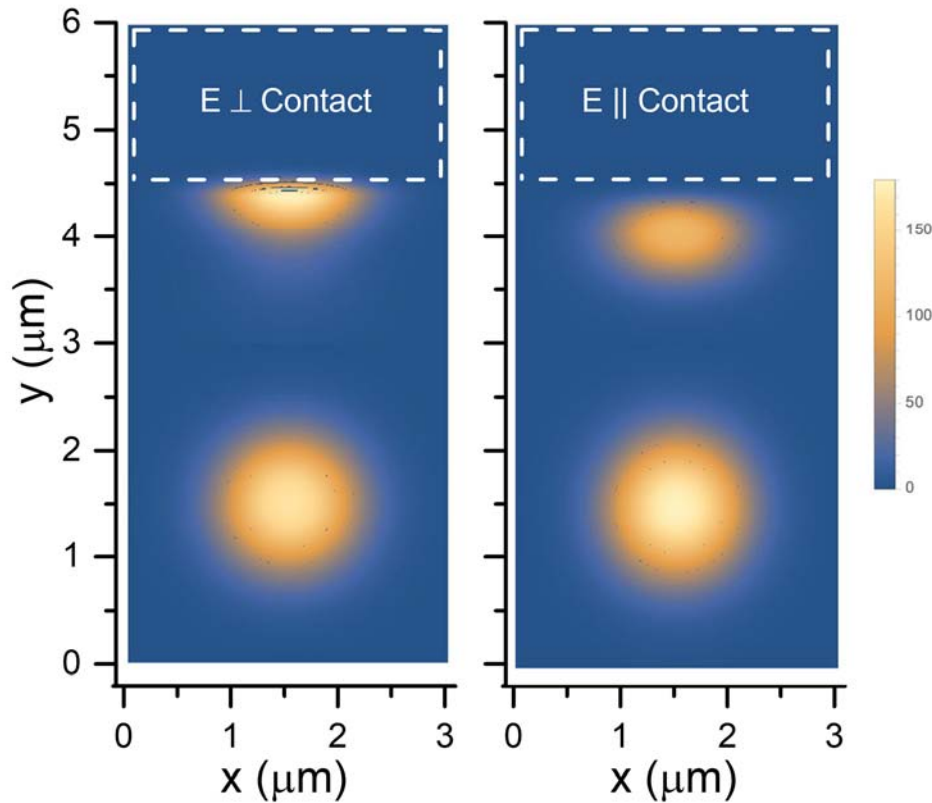


FIG. 4. FDTD Calculation of the square of the electric field E^2 for a linearly polarized 1070 nm laser beam focused to a spot on a Bi_2Se_3 nanoflake device. The left panel shows the field intensity for incident light polarized

perpendicular to the Ti/Al contact, while the right panel shows the field intensity for light polarized parallel to the contact. When the spot is focused well away from the contact the field intensities for each polarization are the same. When light is focused on the Ti/Al metallic contact the intensity is enhanced for perpendicularly polarized light and depleted for parallel polarized light.

In summary, we have shown that it is possible to use the photothermoelectric effect to directly measure the energy dependence of the absorption in a Bi_2Se_3 nanoflake device. We see spectral features that are associated with well-known allowed optical transitions between the valence bands and the conduction bands and are consistent with transient reflectivity measurements on the same material.¹⁵ In addition, we see a peak in the response at 1.5 eV associated with direct optical transitions between the two topologically protected surface states in this well-known topological insulator. While the symmetry of Bi_2Se_3 suggests it should not show any absorption polarization dependence in our geometry, we find a strong linear dichroism for light which is focused on the metal contact of the device. We show through direct FDTD calculations that this strong linear dichroism effect is caused by the expected boundary conditions at the contact interface, which slightly enhances the absorption of the perpendicular polarization and depletes the parallel polarization. These results show that it is possible to measure the optical transitions even in very conductive materials through PTE spectroscopy, but that the presence of contacts can strongly impact their polarization response even when the material is expected to be isotropic. This perhaps opens the possibility to design the contacts to enhance the polarization response of a number of quantum materials.

We acknowledge the financial support of the NSF through grants DMR 1507844, DMR 1531373, and ECCS 1509706. SDW acknowledges support via the UC Santa Barbara NSF Quantum Foundry funded via the Q-AMASE-i program under award DMR-1906325.

Data Availability

The data that support the findings of this study are available from the corresponding author upon reasonable request.

References:

- (1) McIver, J. W.; Hsieh, D.; Steinberg, H.; Jarillo-Herrero, P.; Gedik, N. Control over Topological Insulator Photocurrents with Light Polarization. *Nature Nanotechnology* **2012**, *7* (2), 96–100. <https://doi.org/10.1038/nnano.2011.214>.
- (2) Wang, Y. M.; Yu, J. L.; Zeng, X. L.; Chen, Y. H.; Liu, Y.; Cheng, S. Y.; Lai, Y. F.; Yin, C. M.; He, K.; Xue, Q. K. Temperature and Excitation Wavelength Dependence of Circular and Linear Photogalvanic Effect in a Three Dimensional Topological Insulator Bi₂Se₃. *Journal of Physics Condensed Matter* **2019**, *31* (41). <https://doi.org/10.1088/1361-648X/ab2b55>.
- (3) Yu, J.; Zeng, X.; Zhang, L.; He, K.; Cheng, S.; Lai, Y.; Huang, W.; Chen, Y.; Yin, C.; Xue, Q. Photoinduced Inverse Spin Hall Effect of Surface States in the Topological Insulator Bi₂Se₃. *Nano Letters* **2017**, *17* (12), 7878–7885. <https://doi.org/10.1021/acs.nanolett.7b04172>.
- (4) Kastl, C.; Karnetzky, C.; Karl, H.; Holleitner, A. W. Ultrafast Helicity Control of Surface Currents in Topological Insulators with Near-Unity Fidelity. *Nature Communications* **2015**, *6*, 1–6. <https://doi.org/10.1038/ncomms7617>.
- (5) Besbas, J.; Banerjee, K.; Son, J.; Wang, Y.; Wu, Y.; Brahlek, M.; Koirala, N.; Moon, J.; Oh, S.; Yang, H. Helicity-Dependent Photovoltaic Effect in Bi₂Se₃ Under Normal Incident Light. *Advanced Optical Materials* **2016**, *4* (10), 1642–1650. <https://doi.org/10.1002/adom.201600301>.
- (6) Luo, S. Infrared Circular Photogalvanic Effect in Topological Insulators. *AIP Conference Proceedings* **2018**, *1955* (April). <https://doi.org/10.1063/1.5033750>.
- (7) Fan, D.; Hobara, R.; Akiyama, R.; Hasegawa, S. Inverse Spin Hall Effect Induced by Asymmetric Illumination of Light on Topological Insulator Bi₂Se₃. *arXiv* **2018**, *023055* (March), 1–10. <https://doi.org/10.1103/physrevresearch.2.023055>.
- (8) Liu, Y.; Besbas, J.; Wang, Y.; He, P.; Chen, M.; Zhu, D.; Wu, Y.; Lee, J. M.; Wang, L.; Moon, J.; et al. Direct Visualization of Current-Induced Spin Accumulation in Topological Insulators. *Nature Communications* **2018**, *9* (1). <https://doi.org/10.1038/s41467-018-04939-6>.
- (9) Osterhage, H.; Gooth, J.; Hamdou, B.; Gwozdz, P.; Zierold, R.; Nielsch, K. Thermoelectric Properties of Topological Insulator Bi₂Te₃, Sb₂Te₃, and Bi₂Se₃ Thin Film Quantum Wells. *Applied Physics Letters* **2014**, *105* (12). <https://doi.org/10.1063/1.4896680>.
- (10) Sun, G. L.; Li, L. L.; Qin, X. Y.; Li, D.; Zou, T. H.; Xin, H. X.; Ren, B. J.; Zhang, J.; Li, Y. Y.; Li, X. J. Enhanced Thermoelectric Performance of Nanostructured Topological Insulator Bi₂Se₃.

Applied Physics Letters **2015**, *106* (5), 1–5. <https://doi.org/10.1063/1.4907252>.

- (11) Takahashi, R.; Murakami, S. Thermoelectric Transport in Perfectly Conducting Channels in Quantum Spin Hall Systems. *Physical Review B - Condensed Matter and Materials Physics* **2010**, *81* (16), 1–4. <https://doi.org/10.1103/PhysRevB.81.161302>.
- (12) Ghaemi, P.; Mong, R. S. K.; Moore, J. E. In-Plane Transport and Enhanced Thermoelectric Performance in Thin Films of the Topological Insulators Bi₂Te₃ and Bi₂Se₃. *Physical Review Letters* **2010**, *105* (16), 1–4. <https://doi.org/10.1103/PhysRevLett.105.166603>.
- (13) Tretiakov, O. A.; Abanov, A.; Murakami, S.; Sinova, J. Large Thermoelectric Figure of Merit for Three-Dimensional Topological Anderson Insulators via Line Dislocation Engineering. *Applied Physics Letters* **2010**, *97* (7). <https://doi.org/10.1063/1.3481382>.
- (14) Zhang, Y.; Hapenciuc, C. L.; Castillo, E. E.; Borca-Tasciuc, T.; Mehta, R. J.; Karthik, C.; Ramanath, G. A Microprobe Technique for Simultaneously Measuring Thermal Conductivity and Seebeck Coefficient of Thin Films. *Applied Physics Letters* **2010**, *96* (6), 1–4. <https://doi.org/10.1063/1.3300826>.
- (15) Jnawali, G.; Linser, S.; Shojaei, I. A.; Pournia, S.; Jackson, H. E.; Smith, L. M.; Need, R. F.; Wilson, S. D. Revealing Optical Transitions and Carrier Recombination Dynamics within the Bulk Band Structure of Bi₂Se₃. *Nano Letters* **2018**, *18* (9), 5875–5884. <https://doi.org/10.1021/acs.nanolett.8b02577>.
- (16) Butch, N. P.; Kirshenbaum, K.; Syers, P.; Sushkov, A. B.; Jenkins, G. S.; Drew, H. D.; Paglione, J. Strong Surface Scattering in Ultrahigh-Mobility Bi₂Se₃ Topological Insulator Crystals. *Physical Review B - Condensed Matter and Materials Physics* **2010**, *81* (24), 3–6. <https://doi.org/10.1103/PhysRevB.81.241301>.
- (17) Chiatti, O.; Riha, C.; Lawrenz, D.; Busch, M.; Dusari, S.; Sánchez-Barriga, J.; Mogilatenko, A.; Yashina, L. V.; Valencia, S.; Ünal, A. A.; et al. 2D Layered Transport Properties from Topological Insulator Bi₂Se₃ Single Crystals and Micro Flakes. *Scientific Reports* **2016**, *6* (December 2015), 1–11. <https://doi.org/10.1038/srep27483>.
- (18) Hong, S. S.; Cha, J. J.; Kong, D.; Cui, Y. Ultra-Low Carrier Concentration and Surface-Dominant Transport in Antimony-Doped Bi₂Se₃ Topological Insulator Nanoribbons. *Nature Communications* **2012**, *3*. <https://doi.org/10.1038/ncomms1771>.
- (19) Buscema, M.; Island, J. O.; Groenendijk, D. J.; Blanter, S. I.; Steele, G. A.; Van Der Zant, H. S. J.; Castellanos-Gomez, A. Photocurrent Generation with Two-Dimensional van Der Waals

- Semiconductors. *Chemical Society Reviews* **2015**, *44* (11), 3691–3718. <https://doi.org/10.1039/c5cs00106d>.
- (20) Lu, X.; Jiang, P.; Bao, X. Phonon-Enhanced Photothermoelectric Effect in SrTiO₃ Ultra-Broadband Photodetector. *Nature Communications* **2019**, *10* (1), 1–7. <https://doi.org/10.1038/s41467-018-07860-0>.
- (21) Gupta, S.; Vijayan, N.; Krishna, A.; Thukral, K.; Maurya, K. K.; Muthiah, S.; Dhar, A.; Singh, B.; Bhagavannarayana, G. Enhancement of Thermoelectric Figure of Merit in Bi₂Se₃ Crystals through a Necking Process. *Journal of Applied Crystallography* **2015**, *48*, 533–541. <https://doi.org/10.1107/S1600576715003350>.
- (22) Lee, P.; Wei, P.; Chen, Y. Thermoelectric Characteristics of A Single-Crystalline Topological Insulator Bi₂Se₃ Nanowire. **2021**, 1–11.
- (23) Navrátil, J.; Horák, J.; Plecháček, T.; Kamba, S.; Lošt'ák, P.; Dyck, J. S.; Chen, W.; Uher, C. Conduction Band Splitting and Transport Properties of Bi₂Se₃. *Journal of Solid State Chemistry* **2004**, *177* (4–5), 1704–1712. <https://doi.org/10.1016/j.jssc.2003.12.031>.
- (24) Zhu, J.; Xia, Y.; Li, G.; Zhou, S.; Wimmer, S.; Springholz, G.; Pashkin, A.; Helm, M.; Schneider, H. Absorption Edge, Urbach Tail, and Electron-Phonon Interactions in Topological Insulator Bi₂Se₃ and Band Insulator (Bi_{0.89}In_{0.11})₂Se₃. *Applied Physics Letters* **2019**, *114* (16), 0–5. <https://doi.org/10.1063/1.5080790>.
- (25) Martinez, G.; Piot, B. A.; Hakl, M.; Potemski, M.; Hor, Y. S.; Materna, A.; Strzelecka, S. G.; Hruban, A.; Caha, O.; Novák, J.; et al. Determination of the Energy Band Gap of Bi₂Se₃. *Scientific Reports* **2017**, *7* (1), 1–5. <https://doi.org/10.1038/s41598-017-07211-x>.
- (26) Kannan, A. G.; Manjulavalli, T. E. Structural, Optical and Electrical Properties of Bi₂Se₃ Thin Films Prepared by Spray Pyrolysis Technique. *International Journal of ChemTech Research* **2015**, *8* (11), 599–606.
- (27) Tu, C. M.; Yeh, T. T.; Tzeng, W. Y.; Chen, Y. R.; Chen, H. J.; Ku, S. A.; Luo, C. W.; Lin, J. Y.; Wu, K. H.; Juang, J. Y.; et al. Manifestation of a Second Dirac Surface State and Bulk Bands in THz Radiation from Topological Insulators. *Scientific Reports* **2015**, *5* (March), 1–8. <https://doi.org/10.1038/srep14128>.
- (28) Sobota, J. A.; Yang, S. L.; Kemper, A. F.; Lee, J. J.; Schmitt, F. T.; Li, W.; Moore, R. G.; Analytis, J. G.; Fisher, I. R.; Kirchmann, P. S.; et al. Direct Optical Coupling to an Unoccupied Dirac Surface State in the Topological Insulator Bi₂Se₃. *Physical Review Letters* **2013**, *111* (13), 1–5.

<https://doi.org/10.1103/PhysRevLett.111.136802>.

- (29) Xu, X.; Gabor, N. M.; Alden, J. S.; Van Der Zande, A. M.; McEuen, P. L. Photo-Thermoelectric Effect at a Graphene Interface Junction. *Nano Letters* **2010**, *10* (2), 562–566. <https://doi.org/10.1021/nl903451y>.